UC-25
LBL-20673
Preprint c.1

Lawrence Berkeley Laboratory
UNIVERSITY OF CALIFORNIA

Materials & Molecular Research Division

RECEIVED
LAWRENCE
BERKELEY LABORATORY

AUG 12 1986

LIBRARY AND
DOCUMENTS SECTION

Submitted to Acta Metallurgica

THE MORPHOLOGICAL STABILITY OF CONTINUOUS INTERGRANULAR PHASES: THERMODYNAMIC CONSIDERATIONS

W.C. Carter and A.M. Glaeser

May 1986

For Reference

Not to be taken from this room

LBL-20673 c.1

Prepared for the U.S. Department of Energy under Contract DE-AC03-76SF00098

DISCLAIMER

This document was prepared as an account of work sponsored by the United States Government. While this document is believed to contain correct information, neither the United States Government nor any agency thereof, nor the Regents of the University of California, nor any of their employees, makes any warranty, express or implied, or assumes any legal responsibility for the accuracy, completeness, or usefulness of any information, apparatus, product, or process disclosed, or represents that its use would not infringe privately owned rights. Reference herein to any specific commercial product, process, or service by its trade name, trademark, manufacturer, or otherwise, does not necessarily constitute or imply its endorsement, recommendation, or favoring by the United States Government or any agency thereof, or the Regents of the University of California. The views and opinions of authors expressed herein do not necessarily state or reflect those of the United States Government or any agency thereof or the Regents of the University of California.

Accepted for publication in Acta Metallurgica **LBL Report #20673**

The Morphological Stability of Continuous Intergranular Phases: Thermodynamic Considerations

by

W. C. Carter and A. M. Glaeser

Department of Materials Science
and Mineral Engineering, and
Materials and Molecular Research Division
Lawrence Berkeley Laboratory
University of California
Berkeley, California 94720

ABSTRACT:

A thermodynamic analysis of the morphological stability of continuous intergranular phases, incorporating the number of bounding grains **n**, and dihedral angle ψ as variables is presented. For each **n**, the minimum thermodynamically unstable wavelength of an infinitesimal amplitude perturbation coincides with the Rayleigh result ($2\pi R_c$) for $\psi = 180°$. For $n = 2$, the ratio $\lambda_{min}/2\pi R_c$ decreases with ψ, approaching a limit of $(0.7)^{\frac{1}{2}}$ as $\psi \to 0°$. For $n \geq 3$, $\lambda_{min}/2\pi R_c$ increases with decreasing ψ and tends to infinity as $\psi \to \pi - (2\pi/n)$, or equivalently as the interface curvature vanishes. For fixed ψ, the stability increases with **n**. Several applications and implications of the analysis are discussed.

1. INTRODUCTION:

Rayleigh presented the first complete analysis of the morphological instability of continuous phases in 1878.[1] As Rayleigh remarked, "[these] phenomena, interesting not only in themselves, but also as throwing light upon others yet more obscure, depend for their explanation upon the transformations undergone by a [cylindrical body] when slightly displaced from its equilibrium configuration and left to itself".[2] The Rayleigh analysis indicates that infinitesimal periodic perturbations with a wavelength λ exceeding $2\pi R$ (the cylinder circumference) will reduce the specific (per unit volume) surface energy, and thus will increase in amplitude. Growth of perturbations with $\lambda > \lambda_{min}$ ($= 2\pi R$) eventually cause the formation of one discrete particle per wavelength increment of cylinder.

Such phenomena continue to be the subject of considerable interest; a wide range of microstructural phenomena involving capillarity-induced shape changes have been analyzed or modelled in terms of the Rayleigh analysis. These include: the stability of lamellar eutectics,[3-5] fibers in composites,[6] and artificially lengthened precipitates,[7,8] the shape evolution of field ion emitter tips,[9,10] healing of cracks introduced by thermal shock,[11,12] as well as by scoring and welding of bicrystals,[13,14] and the stability of the continuous pore phase during sintering of powder compacts.[15,16]

The Rayleigh analysis permits qualitative understanding of many of these phenomena, however, complications arise when the continuous phase is located at a grain boundary. For an intergranular phase, each grain boundary intersection is characterized by some dihedral angle. The

associated deviation from a cylindrical geometry changes both the surface energy per unit volume and the stability condition.

The modifying effect of dihedral angle on the stability of continuous grain boundary phases was recognized by C. S. Smith.[17] In discussing continuous phases along three grain junctions Smith wrote, "If a second phase forming at a grain edge has a dihedral angle against grain boundaries of nearly 180°, it will behave like a cylinder and will certainly break up. If, however, the interphase tension is low in comparison with the adjacent grain boundary tension, the resulting triangular shape becomes stable at longer and longer lengths until, at a dihedral angle of 60° and below, the phase becomes stable at any length of grain edge."

The stability of continuous phases along three grain junctions of tetrakaidecahedral grains has been evaluated by both Beere[18,19] and Tucker and Turnbull.[20] These analyses indicate the important modifying effect of dihedral angle on the condition for intergranular phase continuity. More generally, continuous phases may be situated at (along) the junctions of an arbitrary number of grains. The ensuing analysis quantifies the discussion of Smith by extending Rayleigh's method to continuous phases surrounded by **n** grains with (variable) dihedral angle ϕ. Results indicate the stability condition depends strongly on the intergranular phase geometry (as dictated by the values of **n** and ϕ), and may differ significantly from that of a cylinder.

A complete analysis of morphological instability has two components:[21] a thermodynamic analysis identifying the smallest wavelength (infinitesimal amplitude) perturbation for which the amplitude will increase, and a kinetic analysis determining the

particular wavelength for which perturbation growth is most rapid. In this paper, we present a thermodynamic analysis for nonfaceting surfaces with single-valued interfacial tensions. Possible modifications which may result from surface faceting[22,23] and the implications of the analysis to the kinetics of phase breakdown have been discussed elsewhere.[23] A kinetic analysis is forthcoming.[24]

2. THEORETICAL ANALYSIS: DETERMINATION OF λ_{min}

The ensuing sections describe the assumptions made and procedures used in the analysis. The objectives are the calculation of the surface area and volume of both a perturbed and an unperturbed channel as a function of the number of bounding grains **n**, and the dihedral angle ψ. The results of these calculations are employed to define the condition for thermodynamic stability of a continuous grain boundary phase.

2.1 Geometry

Figure 1 illustrates most of the geometrical parameters relevant to the analysis. Isotropic interfacial energies (grain boundary and interphase) are assumed, i.e., the energy for each type of interface has some unique but constant value. Each interphase boundary will thus have identical curvature, and intersect the adjoining interphase boundaries at a common dihedral angle, ψ. The intergranular phase will display n-fold symmetry. The channel cross-section may be circumscribed by a circle of radius R_c, which intersects all n triple junctions.

Simple geometry yields

$$\frac{\rho R_c}{\sin(\pi/n)} = \frac{\eta R_c}{\cos(\psi/2)} = \frac{-R_c}{\cos(\pi/n + \psi/2)} \qquad (1)$$

If the origin of a polar coordinate system (r-θ) coincides with the circumscribing circle's center

$$r = R_c\left(-\eta\cos\theta + \sqrt{\rho^2 - \eta^2\sin^2\theta}\right) \qquad (2)$$

A perturbation on the cross-section can be described as the largest term of some periodic function of wavelength $\lambda = 2\pi/k$ and arbitrarily small amplitude δ

$$R_c = R_o + \delta \cos kz \tag{3}$$

We may then express r in the form

$$r = r_z r_\theta \tag{4}$$

where r_z and r_θ are functions of z and θ only, respectively.

2.2 Determination of Interfacial Area

The total interfacial area is comprised of a sum of grain boundary area and interphase boundary area contributions. For convenience, the interphase boundary energy may be set equal to unity (in appropriate units), and the grain boundary energy expressed as $(2 \cos \psi/2)$. The total interfacial energy may thus be expressed as

$$F = \sigma_s + \sigma_{gb}(2 \cos \psi/2) \tag{5}$$

where σ_s is the interphase boundary area, σ_{gb} is the grain boundary area. It is convenient to consider the interfacial free energy per wavelength of perturbation

$$f = A_s + A_{gb}(2 \cos \psi/2) \tag{6}$$

where A_{gb} is

$$A_{gb} = n \int_0^{2\pi/k} (\alpha - [R_o + \delta \cos kz])\, dz \tag{7}$$

$$= \frac{2n\pi}{k} (\alpha - Ro) \tag{8}$$

and α is some arbitrary length. Similarly, we may express A_s as

$$A_s = n \int_{-\pi/n}^{\pi/n} d\theta \int_0^{2\pi/k} dz\, [r^2 + (\partial r/\partial\theta)^2 + r^2(\partial r/\partial z)^2]^{\frac{1}{2}} \tag{9}$$

Since dr/dz is of order δ and arbitrarily small, we keep terms of order up to δ^2, yielding

$$A_s \simeq \frac{2n\pi R_o}{k} \int_{-\pi/n}^{\pi/n} d\theta\, [r_\theta^2 + (dr_\theta/d\theta)^2]^{\frac{1}{2}} \left(1 + \frac{\delta^2 k^2 r_\theta^4}{4(r_\theta^2 + (dr_\theta/d\theta)^2)} \right) \tag{10}$$

$$= \frac{2n\pi R_o}{k} (U + \frac{\delta^2 k^2}{4} P) \tag{11}$$

where

$$U = 2\rho(\pi/n + \psi/2 - \pi/2) \tag{12}$$

and

$$\begin{aligned} P = {} & (2\rho^3 + \rho\eta^2)(\pi/n + \psi/2 - \pi/2) + \cos \psi/2\, (5\eta\rho^2 \cos \pi/n \\ & - 2\eta^3 \sin^2 \pi/n \cos \pi/n - \eta^2\rho \sin \psi/2 - 2\rho^3 \sin \psi/2 \\ & - 2\rho^3 \sin^3 \psi/2) \end{aligned} \tag{13}$$

2.3 Volume Determination and Criterion for Break-up

The cross-sectional area of the intergranular phase (channel) is

$$A_{cs} = R_c^2 \, [n \, (\sin \pi/n \cos \pi/n + \rho^2(\psi/2 + \pi/n - \pi/2 + \sin(\pi/n + \psi/2) \cos(\pi/n + \psi/2)))] \tag{14}$$

$$= R_c^2 \, \chi \tag{15}$$

The channel volume per perturbation wavelength is

$$V = \frac{\pi\chi}{k} \, (2R_o^2 + \delta^2) \tag{16}$$

To sufficient approximation

$$R_o = \xi - \frac{\delta^2}{4\xi} \tag{17}$$

where

$$\xi = (kV/2\pi\chi)^{\frac{1}{2}} \tag{18}$$

Combining Eqs. 6, 8, 11, and 17 yields a result expressible in the form

$$f = f_o + \frac{n\pi}{k\xi} \, (2 \cos \psi/2 - U + \xi^2 k^2 P) \, \frac{\delta^2}{2} \tag{19}$$

We may consider Eq. 19 as the expansion of the free energy about a metastable value f_o, by an infinitesimal amount δ. As is the case in all problems of metastability, stability is determined by the sign of the second derivative, i.e., the term multiplying $\delta^2/2$. Thus, the channel is unstable to all infinitesimal perturbations with wavelength $\lambda = 2\pi/k$ for which

$$(2 \cos \psi/2 - U + \xi^2 k^2 P) < 0 \tag{20}$$

This defines a critical condition for perturbation growth. Perturbations with a wavelength exceeding λ_{min}, where*

$$\lambda_{min} = 2\pi R_o \left(\frac{P}{U - 2 \cos \psi/2} \right)^{\frac{1}{2}} \tag{21}$$

decrease the free energy and thus grow (increase in amplitude) without thermodynamic barrier. The $(2 \cos \psi/2)$ term stems from grain boundary area changes. Since dihedral angles $\leq 180°$ are considered, $\cos \psi/2$ is always ≥ 0. For ψ between $\pi - (2\pi/n)$ and π, both U and P are ≥ 0. Thus, the change in grain boundary area accompanying development of a perturbation increases λ_{min} and stabilizes the intergranular phase.

2.4 End-State Calculations

The stability condition derived in this analysis defines the minimum wavelength necessary for an infinitesimal periodic perturbation on $\mathbf{R_c}$ to increase in amplitude. As detailed in Section 2.3, infinitesimal perturbations with $\lambda > \lambda_{min}$ decrease the interfacial energy in comparison to that of an unperturbed cylinder having the same volume per wavelength.

The interfacial area of the perturbed "cylinder" is sensitive to the form of the imposed perturbation. Conceivably, a perturbation with an additional radial or rotational component could yield a smaller λ_{min}

---

*Since we are only concerned with the sign of the Eq. 20, it is sufficient to approximate ξ as R_o.

than derived here. Hence, although the calculated values for λ_{min} presented serve as a **sufficient** condition for instability, perturbations of greater geometrical complexity may provide a smaller value for λ_{min} as a **necessary** condition for instability.

In view of this uncertainty, it is desirable to determine a lower limit wavelength $\lambda_{\ell\ell}$ as a function of **n** and $\boldsymbol{\psi}$. This entails calculating the perturbation wavelength for which the total (grain boundary and interphase boundary) interfacial energy per wavelength in the unperturbed and final (discrete particle) states are equal (Appendix I). Shorter wavelength perturbations would increase total interfacial energy. Thus, the difference between λ_{min} and $\lambda_{\ell\ell}$ indicates the **maximum** possible reduction in λ_{min} achievable by imposition of a more geometrically complex or finite perturbation.

The calculation is straightforward for $\psi = 180°$, since this implies $\gamma_{gb} = 0$, and consequently, changes in grain boundary area accompanying the transition from a cylinder to an ensemble of equidistant spheres of equivalent total volume need not be considered.* For the simple case of a cylinder, $\lambda_{\ell\ell} = 4.5R_c$ independent of **n**. For $\psi < 180°$, the calculation is more tedious. Results for n = 2 and 3 are presented in Figs. 2a and 3a, respectively. For n = 3, results of Clemm and Fisher[25] were used to describe the geometry of the discrete phase. The generalization to arbitrary **n** and results for n > 3 will be presented elsewhere.[24]

---

*Comparison of end-state calculations for n = 2,3 including and excluding grain boundary area changes indicate a trend similar to that suggested by Eq. 21, i.e., the grain boundary area changes associated with an infinitesimal perturbation increase λ, and stabilize the continuous phase.

3. DISCUSSION:

Results of the analysis for several **n** are presented in Figures 2-4. For each **n** (Figures 2a-4a), λ_{min} coincides with the Rayleigh result ($2\pi R_c$) for $\psi = 180°$. For n = 2, the ratio $\lambda_{min}/2\pi R_c$ is <1 for all $\psi < 180°$, decreasing with ψ to a limit of $(0.7)^{\frac{1}{2}}$ as $\psi \to 0°$. The corresponding end state calculation (Section 2.4 and Appendix I) for n = 2 indicates that $\lambda_{\ell\ell}$ follows a similar trend, decreasing from 0.716 at $\psi = 180°$ to 0.633 when $\psi \to 0°$. The present values of $\lambda_{min}/2\pi R_c$ are lower than those appropriate to a sinusoidal perturbation imposed on ρ,[23] and thus more closely approach a **necessary** condition for instability. The close correspondence between λ_{min} and $\lambda_{\ell\ell}$ suggests that although a further reduction in λ_{min} is possible, the decrease is likely to be small.

For **n** ≥ 3, λ_{min} and $\lambda_{min}/2\pi R_c$ tend to infinity as $\psi \to \pi - (2\pi/n)$, or equivalently, as the interface curvature vanishes. The end state calculation (n = 3) shows a similar increase in $\lambda_{\ell\ell}$ as ψ decreases from 180° to 60°. A previous analysis indicated a similar trend but a more rapid increase in $\lambda_{min}/2\pi R_c$ with decreasing ψ.[23] For fixed **n**, a continuous phase with lower ψ is expected to be more stable than one with higher ψ. For n $\geq$ 3, the phase is completely stable to (infinitesimal) perturbations when $\psi \leq \pi - (\pi/2n)$. For fixed ψ, the stability increases with **n** (Table I).

To facilitate comparison between this analysis and that of Rayleigh, two normalization parameters are introduced. Defining R_{eq} as the cylinder radius yielding the same volume per unit length as an intergranular phase characterized by a dihedral angle ψ, the ratio

$\lambda_{min}/2\pi R_{eq}$ normalizes the actual λ_{min} by the minimum wavelength that would grow in a geometrically similar compact with an equivalent volume fraction of (cylindrical) second phase. The dependence of $\lambda_{min}/2\pi R_{eq}$ on ψ for various **n** is presented in Figs. 2b-4b.

An alternative normalization mode is based on consideration of the surface curvature as characterized by ρ. The stability condition of the intergranular phase may be compared with that of a cylinder having the same curvature, i.e., one with a radius ρ. The results of this comparison, presented in Figs. 2c-4c, indicate that the approximation $\lambda_{min} \approx 2\pi\rho$ overestimates λ_{min} for all $\psi < 180°$ and becomes progressively poorer as ψ decreases.*

3.1 General Considerations:

The composition, inherent properties, morphology, and spatial distribution of a second phase within a matrix, can have an important impact on a material's ultimate properties. The incorporation of continuous filaments into polycrystalline matrices may dramatically alter mechanical behavior. High temperature stability and useful lifetimes of such composites will be influenced by the fibers' relative susceptibility to morphological instabilities and concurrent coarsening.[3] Continuous phases may provide high diffusivity transport paths, (e.g., vapor transport along continuous pore channels in UO_2 fuel elements[20]) or be preferentially leached, thus limiting the utility of a material in storage applications, e.g., containment of nuclear waste.

---

*In comparing normalizations, the trend $\lambda/2\pi\rho < \lambda/2\pi R_c < \lambda/2\pi R_{eq}$ is simply a consequence of having $\rho > R_c > R_{eq}$ when $\psi < 180°$.

In these cases as well as others, factors influencing the morphological stability of continuous phases may become important considerations in materials design. In the following, a number of specific cases are considered, and the extent to which dihedral angle may stabilize an intergranular phase is indicated.

3.2 Consideration of n = 2

Crack healing experiments have been conducted on cracked sapphire single crystals,[13] bicrystals,[14] and thermally shocked polycrystals[11] and used to determine surface diffusivities in alumina. During annealing, the crack first breaks down into parallel, high aspect ratio pore channels. These channels in turn undergo a Rayleigh instability, resulting in breakup into a string of equidistant isolated pores. The ratio of pore spacing (λ) to (apparent) pore radius r_p is used to distinguish between surface diffusion and volume diffusion controlled breakup, while the pore radius r_p and an experimentally measured breakup (ovulation) time are used to determine the appropriate diffusivity.

The dihedral angle will affect the shapes of both the continuous and discrete pores, and through its effect on λ_{min}, will also affect the kinetically dominant wavelength, and thus both the size and spacing of discrete particles or phases resulting from perturbation growth processes. Experiments on a series of bicrystals with a systematic variation in ψ (owing to misorientation effects) would be expected to reveal a systematic variation in particle size and spacing. In polycrystals, incorporating a spectrum of ψ, "scatter" in the sizes and spacings of discrete particles would be observed. In polycrystalline alumina,[11] the pore spacing to pore diameter **ratio** varied by as much as

factor two. Similar variability was obtained for the breakdown of elongated bubbles (appearing to lie on two grain interfaces) in tungsten filaments.[8]

For alumina, surface diffusion was identified as the dominant transport process in each case. However, the deduced surface diffusivities differ by between one and two orders of magnitude at the same temperature. An assessment of the contribution to scatter owing to dihedral angle effects is therefore of interest.

Since the shapes of both the pore channel and the isolated pores are affected by ψ, it is anticipated that $\lambda/2r_p$ will also be dihedral angle dependent. For constant λ/R_c, $\lambda/2r_p$ decreases by ≈4% as ψ varies from 180° to 0° (Appendix II). Recent dihedral angle measurements in alumina by Handwerker[26] have indicated a wide dihedral angle range, 85° to 170°. Within this range of ψ, there is a factor ≈1.14 decrease in λ_{min}. The total "scatter" in $\lambda/2r_p$ will depend on the dihedral angle dependence of the kinetically dominant wavelength. If the kinetically dominant wavelength is a mechanism dependent, but dihedral angle independent multiple of λ_{min}, the total scatter in $\lambda/2r_p$ owing to dihedral angle effects is <±10% and similar $\lambda/2r_p$ ratios would be obtained regardless of whether measurements were conducted on single crystals or polycrystals. If the observed scatter reflects primarily dihedral angle effects, the ratio of the kinetically dominant wavelength to λ_{min} must depend on ψ.

While the pore spacing:pore diameter **ratio** is used to determine the dominant transport <u>mechanism</u>, the appropriate diffusivity is calculated using the measured breakdown time and the isolated pore's radius. For surface diffusion dominated breakdown of a cylindrical pore, the

breakdown time is proportional to r^4/D_s. Only when $\psi = 180°$ is the isolated pore spherical and the analysis strictly valid. For a lenticular pore on a two grain interface, r_p, the apparent pore radius, is both proportional to $\lambda^{\frac{1}{2}}$ and a function of ψ. The breakdown time will also be modified by dihedral angle effects on both local curvature differences and the volume of mass which must be transported to accomodate breakdown. Discrepancies between surface diffusivities determined using single crystals and polycrystals are thus likely. A quantitative assessment of these effects is in progress.[24]

3.3 Consideration of n = 3

Pore stability during intermediate stage sintering has been considered by Beere,[18,19] Tucker and Turnbull,[20] as well as others. Two approaches have been employed. Beere, and Tucker and Turnbull have assumed a specific grain shape, a tetrakaidecahedron, and evaluated the pore shape minimizing the total interfacial energy (at constant density) as a function of ψ. The results indicate that the compact density at which a continuous pore phase (along three grain junctions) is no longer stable increases as ψ decreases. Pore phase breakdown is predicted at a pore fraction of ≈8% when $\psi = 180°$, and a pore fraction approaching 0% as $\psi \rightarrow 60°$. For UO_2, for which $\psi \approx 90°$ is quoted, the critical porosity is ≈4%. Similar values are presented by Tucker and Turnbull.

Alternatively, the pore phase has been approximated as a cylindrical channel along three grain junctions. Breakdown of the continuous pore phase, marking the transition from intermediate to final stage sintering, has been assumed to occur by perturbation growth processes. Assuming the same grain shape as Beere, and equating the

grain edge length to λ_{min}, one can similarly estimate the critical density at which pore closure could occur by a Rayleigh instability. The volume fractions porosity corresponding to ψ = 180°, 90° and 60° are ≈8%, 2%, and 0% respectively. Although this approach neglects "end effects" associated with four grain corners, a similar trend in stability and critical pore fraction are indicated; a decrease in ψ is expected to delay pore closure until a higher density has been reached. The dihedral angle distribution may consequently have an important modifying effect on microstructural evolution.

Nichols has recently presented a simplified model for stable open porosity in which pores are idealized as cylinders, predicting a critical volume fraction of porosity (or swelling) of ≈5-6% for the continuous/discontinuous porosity transition for equiaxed grains.[27] A dihedral angle distribution would be expected to introduce a **spectrum** of transition conditions, with pore channels of higher ψ closing more rapidly and at lower density. The gradual loss of (redundant) open pore channels makes gas removal (e.g., binder burnout) more difficult. Eventually, regions will become isolated from the surface due to the closure of lower ψ channels. Pore phase continuity will also affect the swelling of ceramic nuclear fuels. During swelling, low ψ channels would be expected to open first, and venting of gases should occur when adequate pore interconnectivity is achieved.

Dihedral angle distribution dependent spectra of pore closure conditions and sizes, will also introduce a spectrum of pore-grain boundary separation conditions. This factor, combined with effects of ψ on pore shrinkage and coarsening behavior, as well as pore mobility,[28]

may contribute to the development of microstructural inhomogeneities promoting the initiation of abnormal grain growth.

Narrowing the dihedral angle distribution would be expected to lead to more uniform microstructure development. A comparison of dihedral angle measurements in undoped and MgO-doped Al_2O_3,[26] has indicated that dopant additions reduce the width of the dihedral angle distribution. Handwerker et al. point out this increases the uniformity of microstructural evolution by reducing the variation in driving forces for densification.[29] The potential benefits of a dopant-induced reduction in boundary mobility have frequently been cited. Dopant effects on the uniformity of the pore structure produced during the transition from intermediate to final stage sintering may also be important.

In addition to the pore phase in powder compacts, second phases at three-grain junctions are commonly found in alloys with a large difference in either the melting points or solubilities of the constituents.[17] A residual glassy phase along three-grain junctions may also develop in liquid-phase sintered materials. Similar stabilizing effects may be of importance in these cases as well.

3.4 Consideration of $n \geq 4$

Table I illustrates the increased stability to perturbation growth accompanying an increase in **n** (ψ constant). The enhanced stability is manifested in two ways. The stabilizing effect becomes significant at progressively higher ψ as **n** increases, and the dihedral angle range within which perturbation growth is possible diminishes (Figs. 2-4).

Thus, stabilization effects of the type considered are expected to be extremely important when a continuous phase is bounded by a large number of grains.

When **n** is large, one would also anticipate periodic fiber-matrix grain boundary intersections along the fiber axis, and "rumpling" of the fiber surface in the z direction. The resulting changes in the geometry of both the unperturbed reference state and the perturbed state are expected to modify λ_{min}. Growth of a perturbation results in a net increase in grain boundary area and enhances stability (Eq. 21). Increasing grain boundary density is thus expected to increase λ_{min}. The extent to which λ_{min} is increased by this effect increases as ψ decreases, perhaps as much as doubling λ_{min} as $\psi \rightarrow \pi - (2\pi/n)$. When $\psi < 180°$, surface rumpling will also modify λ_{min}, however, a quantitative assessment is difficult.

The general trend illustrated in Table I suggests that the high temperature stability of intergranular phases could be enhanced by proper manipulation of ψ and **n**. If stability to breakdown were desirable, e.g., fibers in composites, it would be advantageous to maximize the number of coordinating grains. Thus grain size:fiber diameter ratio (**Q**) emerges as a potentially important parameter in materials design.

Grain growth and fiber coarsening may modify **n**, introducing an additional time-dependent component to morphological stability. Grain growth may dramatically decrease fiber stability within certain ranges of **Q**. A decrease in **Q** from 20 to 4 may only have a limited effect, whereas an additional factor of 2-3 increase in grain size would likely have a profound influence on fiber stability.

When **n** is sufficiently large to inhibit perturbation growth, other factors inducing mass redistribution along or between fibers may assume greater significance. A "perturbation" or variation in **n** along the fiber axis will produce local curvature differences which may induce mass transfer from regions of lower n to higher-n regions; relatively coarse-grained regions may emerge as preferential fiber-pinchoff sites. Similarly, differences in coordination number may provide a driving force for interfiber mass transfer (coarsening).

Cline has proposed that if the rod fraction in a composite exceeds 20%, two-dimensional coarsening occurs more rapidly than breakdown and spheroidization.[3] Weatherly has proposed a lower volume fraction for this transition.[5] These estimates are likely to be further modified when intergranular phases are considered. The minimum aspect ratio necessary for breakdown into two or more particles will increase as **n** increases and/or ψ decreases. Local surface curvatures, and thus the curvature differences driving coarsening are also affected by **n** and ψ. Thus, analysis of transition conditions appropriate to intergranular phases is likely to be complex.

Acknowledgements:

This work was supported by the Office of Energy Research, Office of Basic Energy Sciences, Materials Sciences Division of the U. S. Department of Energy under Contract No. DE-AC03-76SF00098. One of the authors (WCC) was supported in part by an ARCO Foundation Fellowship. J. W. Cahn, R. M. Cannon, F. A. Nichols, L. Sadun and J. Salmon are thanked for helpful discussions and comments. Finally, we wish to acknowledge the enthusiastic support of G. O. Bears.

Appendix I: End-State Calculation

It is useful to determine the size of the discrete particle, resulting from the breakup of a continuous phase, which yields the same total interfacial energy as the original unperturbed continuous phase. The calculated size defines an absolute lower limit for the wavelength of breakup, independent of the perturbation details. A sample calculation for n = 2 is presented below.

Using parameters defined in Section 2.2, the volume of the continuous phase assumes the form

$$V_c = [R_o^2\lambda(\psi - \sin\psi)]/\sin^2(\psi/2). \qquad \text{(I-1)}$$

The total interfacial energy is given by

$$f_c = (\alpha - R_o)\lambda(4\cdot\cos\psi/2) + \lambda R_o(2\psi/\sin\psi/2). \qquad \text{(I-2)}$$

The volume of the discrete phase is

$$V_d = 2\pi r^3(1 - \cos\psi/2)^2(2 + \cos\psi/2)/3 \qquad \text{(I-3)}$$

where r is the radius of curvature of the spherical cap. The total interfacial energy for the discrete phase is

$$f_d = (2\alpha\lambda - \pi r^2\sin^2\psi/2)(2\cos\psi/2) + 4\pi r^2(1 - \cos\psi/2) \qquad \text{(I-4)}$$

Volume conservation requires that $V_c = V_d$. The lower limit wavelength $\lambda_{\ell\ell}$ is thus defined by setting $f_c = f_d$, yielding

$$\frac{\lambda_{\ell\ell}}{2\pi R_o} = \frac{9\ (2(1 - \cos\psi/2) - \cos\psi/2\ \sin^2\psi/2)^3}{(8\ \sin\psi/2)(\psi - \sin\psi)(2 + \cos\psi/2)^2(1 - \cos\psi/2)^4} \qquad \text{(I-5)}$$

The limit of $\lambda_{\ell\ell}/2\pi R_o$ as ψ approaches 0° is $(3^4/2^7) \approx 0.6328$.

Appendix II: Effect of ψ on $\lambda/2r_p$

Crack healing experiments have been employed to estimate the surface diffusivity of alumina. The transport mechanism controlling breakdown of high aspect ratio pore channels is determined by evaluating the pore spacing:pore diameter ratio. An analysis of dihedral angle effects on this ratio for n = 2 follows.

The volume conservation condition $V_c = V_d$ (Appendix I) provides a relationship between R_o and r. The spacing between pore centers is simply λ. The apparent (grain boundary plane) pore radius r_p is related to the radius of curvature of the spherical cap r by

$$r_p = r \cdot \sin \psi/2 \qquad \text{(II-1)}$$

If the perturbation wavelength is expressed as

$$\lambda = k \cdot 2\pi R_o \qquad \text{(II-2)}$$

where k is a kinetic scaling factor, the ratio $\lambda/2r_p$ is of the form

$$\lambda/2r_p = (2.178) \cdot k^{2/3} \cdot G^{1/3} \qquad \text{(II-3)}$$

where

$$G = \left(\frac{2 - 3 \cdot \cos \psi/2 + \cos^3 \psi/2}{\sin \psi/2 \, (\psi - \sin \psi)} \right) \qquad \text{(II-4)}$$

Consequently, to assess the changes in $\lambda/2r_p$ that are purely the consequence of changes in phase geometry, one can evaluate the change in $G^{1/3}$ as ψ varies from 180° to 0°. The results are tabulated below.

ψ	180°	160°	140°	120°	100°
$G^{1/3}$	0.860	0.850	0.843	0.838	0.833

ψ	80°	60°	40°	20°	0°
$G^{1/3}$	0.830	0.828	0.827	0.826	0.82548

References:

1. Lord Rayleigh, "On the Instability of Jets," Proc. London Math. Soc., 10, 4-13 (1879).

2. Lord Rayleigh, Theory of Sound, Vol. 2, 2nd Edition, MacMillan and Co., London, (1929).

3. H. E. Cline, "Shape Instabilities of Eutectic Composites at Elevated Temperatures," Acta Metall., 19, [6], 481-90 (1971).

4. T. H. Courtney, "Thermal and Mechanical Stability in Finely Divided Structures," in New Developments and Applications in Composites, edited by D. Kuhlmann-Wilsdorf and W. C. Harrison Jr., Met. Soc. of the AIME, Warrendale PA, 1979, pp. 1-30.

5. G. C. Weatherly, "The Stability of Eutectic Microstructures at Elevated Temperatures," pp. 121-75 in Treatise on Materials Science and Technology, Vol. 8, (Academic Press, New York) (1975).

6. A. J. Stapley and C. J. Beevers, "The stability of sapphire whiskers in nickel at elevated temperatures, Part 2," J. Mater. Sci., 8, 1296-1306 (1973).

7. M. McLean, "The kinetics of spheroidization of lead inclusions in aluminium," Philos. Mag., 27, 1253-66 (1973).

8. D. M. Moon and R. C. Koo, "Mechanism and Kinetics of Bubble Formation in Doped Tungsten," Met. Trans., 2, [8], 2115-22 (1971).

9. F. A. Nichols and W. W. Mullins, "Surface (Interface) and Volume-Diffusion Contributions to Morphological Changes Driven by Capillarity," Trans. A.I.M.E., 233, [10], 1840-48 (1965).

10. F. A. Nichols and W. W. Mullins, "Morphological Changes of a Surface of Revolution due to Capillarity-Induced Surface Diffusion," J. Appl. Phys., 36, [6], 1826-35 (1965).

11. T. K. Gupta, "Instability of Cylindrical Voids in Alumina," J. Am. Ceram. Soc., 61, [5-6], 191-95 (1978).

12. T. K. Gupta, "Crack Healing in Thermally Shocked MgO," ibid., 58, [3-4], 143 (1975).

13. C. F. Yen and R. L. Coble, "Spheroidization of Tubular Voids in Al_2O_3 Crystals at High Temperatures," ibid., 55, [10], 507-09 (1972).

14. O. Maruyama and W. Komatsu, "Observations on the Grain-Boundary of Al_2O_3 Bicrystals," Ceramurgica International, 5, [2], 51-5 (1979).

15. W. C. Carter and A. M. Glaeser, "Dihedral Angle Effects on the Stability of Pore Channels," J. Am. Ceram. Soc., 67, [6], C124-C127 (1984).

16. M. D. Drory and A. M. Glaeser, "The Stability of Pore Channels: Experimental Observations," ibid., 68, [1], C14-C15 (1985).

17. C. S. Smith, "Grains, Phases, and Interfaces: An Interpretation of Microstructure," Trans. A.I.M.E., 175, [1], 15-51 (1948).

18. W. Beere, "A Unifying Theory of the Stability of Penetrating Liquid Phases and Sintering Pores," Acta Metall., 23, [1], 131-8 (1975).

19. W. Beere, "The sintering and morphology of interconnected porosity in UO_2 powder compacts," J. Mat. Sci., 8, [12], 1717-24 (1973).

20. M. O. Tucker and J. A. Turnbull, "The morphology of interlinked porosity in nuclear fuels," Proc. R. Soc. Lond. A. 343, 299-314 (1975).

21. F. A. Nichols, "On the Spheroidization of Rod-Shaped Particles of Finite Length," J. Mater. Sci., 11, [6], 1077-82 (1976).

22. J. W. Cahn, "Stability of Rods with Anisotropic Surface Free Energy," Scripta Metall., 13, [11], 1069-71 (1979).

23. W. C. Carter and A. M. Glaeser, "The Morphological Stability of Continuous Intergranular Phases," to be published in Proceedings of the Twenty-First University Conference on Ceramic Science, Penn State University, July 17-19, 1985 (also LBL Report #19'60).

24. W. C. Carter and A. M. Glaeser, to be published

25. P. J. Clemm and J. C. Fisher, "The Influence of Grain Boundaries on the Nucleation of Secondary Phases," Acta Metall., 3, [1], 70- 73 (1955).

26. C. A. Handwerker, "Sintering and Grain Growth in MgO"; Sc.D. Thesis, Massachusetts Institute of Technology, Cambridge, MA, February 1983.

27. F. A. Nichols, "A Simplified Model for Stable Open Porosity," submitted to J. Am. Ceram. Soc..

28. C. H. Hsueh, A. G. Evans, and R. L. Coble, "Microstructure Development During Final/Intermediate Stage Sintering - I. Pore/Grain Boundary Separation," Acta Metall., 30, [7], 1269-79 (1982).

29. C. A. Handwerker, R. M. Cannon, and R. L. Coble, "Final Stage Sintering of MgO," pp. 619-43 in Structure and Properties of MgO and Al_2O_3 Ceramics, Vol. 12 in Advances in Ceramics, W. D. Kingery, Ed., ACS Publication (1984).

Figure Captions:

Figure 1 Geometry of intergranular phase, and illustration of parameters ρ, η, R_c, and dihedral angle ψ. (XBL861-7403)

Figure 2 Effect of dihedral angle on normalized λ_{min} for n = 2. Wavelengths are normalized with respect to (a) $2\pi R_c$, (XBL866-2327) (b) $2\pi R_{eq}$ where R_{eq} is the radius of a cylinder having equivalent volume per unit length (XBL866-2328), and (c) $2\pi\rho$, where ρ is the curvature (XBL866-2329).

Figure 3 Effect of dihedral angle on normalized λ_{min} for n = 3. Normalization parameters are as described for Figure 2. At $\psi \leq 60°$ (shading) the phase is stable to perturbations of infinite wavelength. [a-(XBL866-2330), b-(XBL866-2332), c-(XBL866-2331)]

Figure 4 Effect of dihedral angle on normalized λ_{min} for n = 4 and 6, illustrating the rapid increase in normalized λ_{min} as n increases. Normalization parameters are as described for Figure 2. [a-(XBL866-2333), b-(XBL866-2334), c-(XBL866-2335)]

Table Captions:

Table I Comparison of $\lambda/2\pi R_c$, $\lambda/2\pi\rho$, and $\lambda/2\pi R_{eq}$ for $\psi = 135°$ and n varying from 2 to 8.

Table I

$\psi = 135°$

n	$\lambda_{min}/2\pi R_c$	$\lambda_{min}/2\pi\rho$	$\lambda_{min}/2\pi R_{eq}$
2	0.910	0.841	1.161
3	1.093	0.768	1.266
4	1.271	0.688	1.415
5	1.500	0.596	1.633
6	1.864	0.487	2.000
7	2.663	0.344	2.824
8	∞	-0-	∞

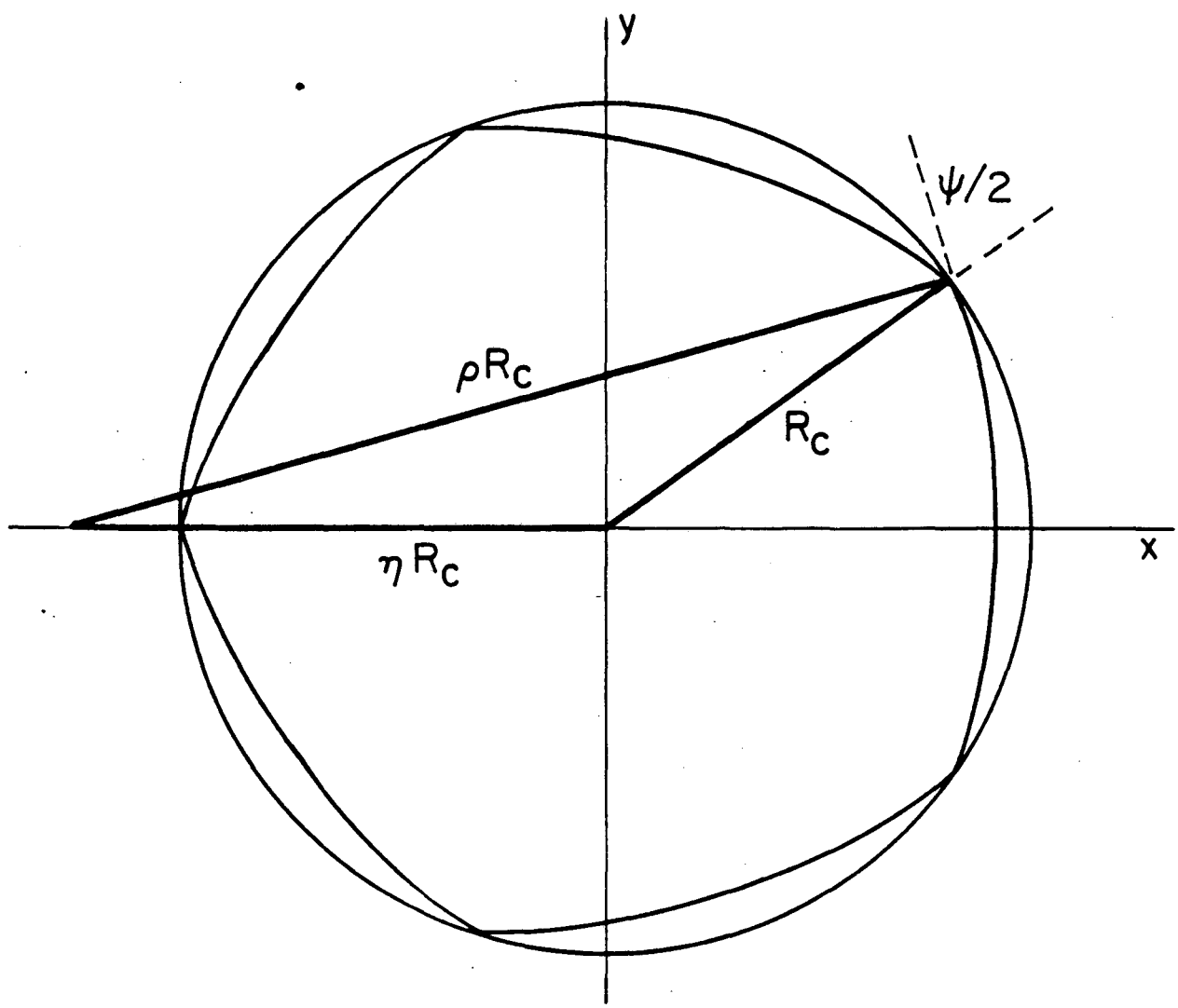

XBL861-7403

Figure 1

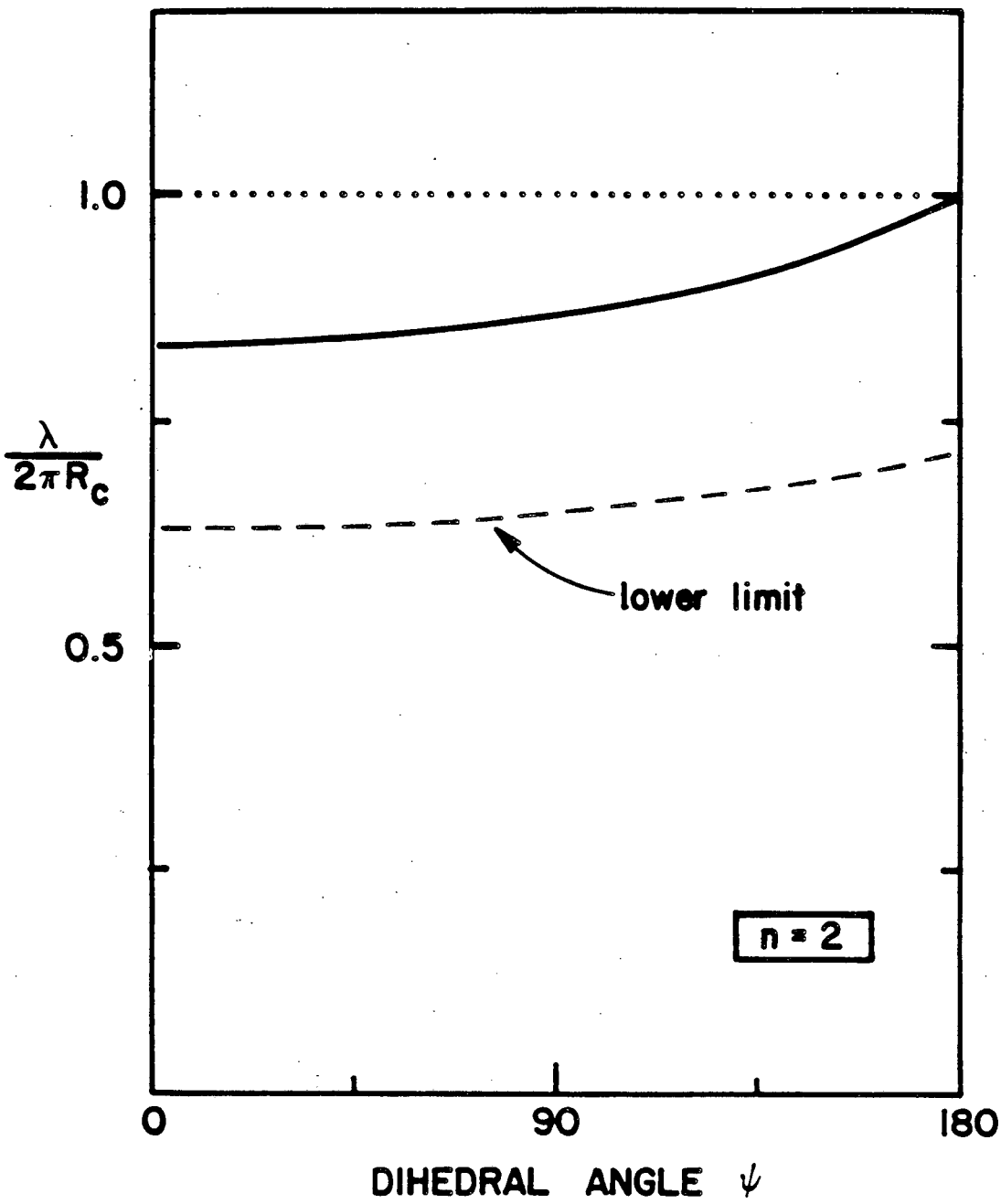
1.0
0.5
$\frac{\lambda}{2\pi R_c}$
lower limit
n = 2
0
90
180
DIHEDRAL ANGLE ψ

Figure 2a

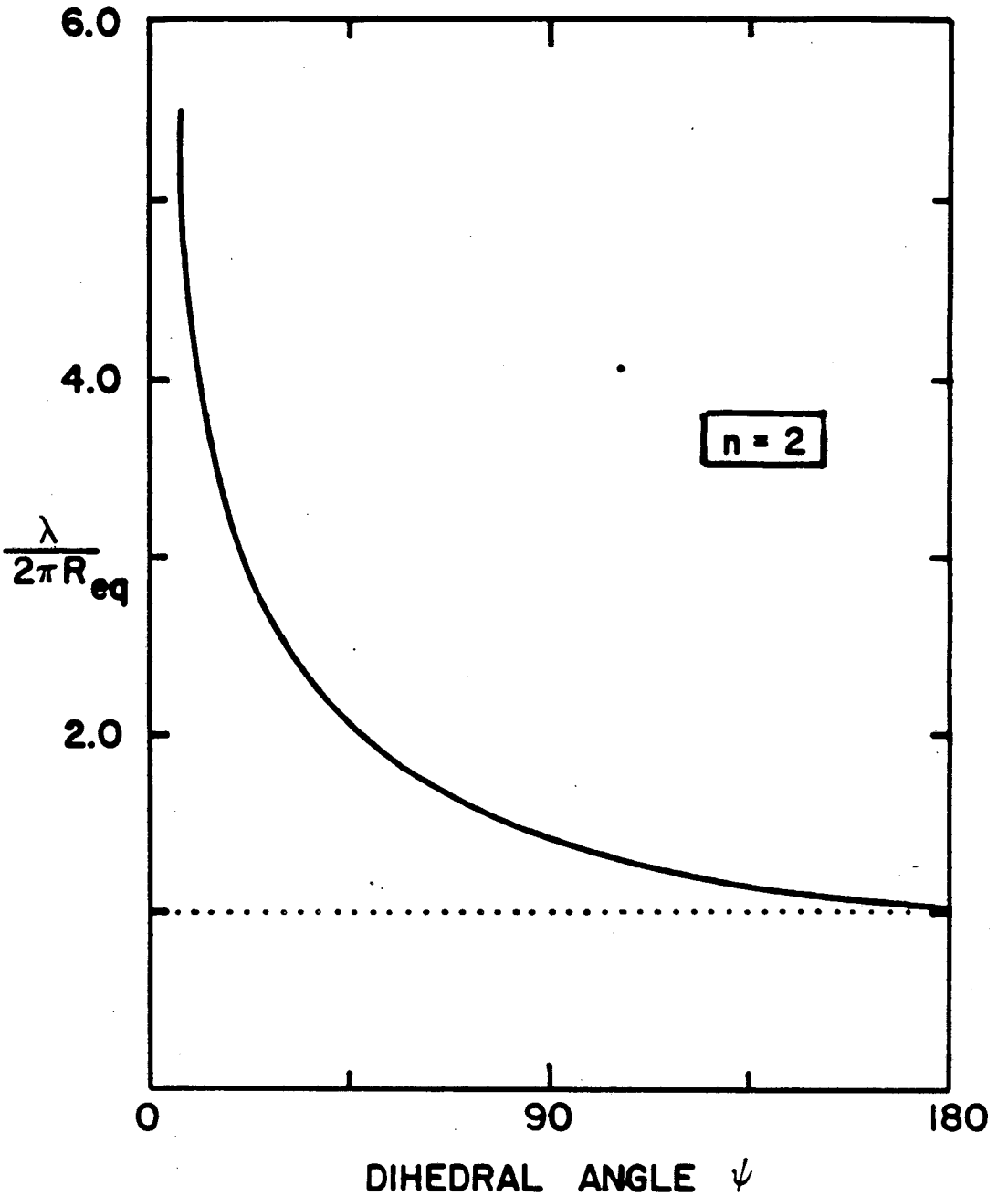

Figure 2b

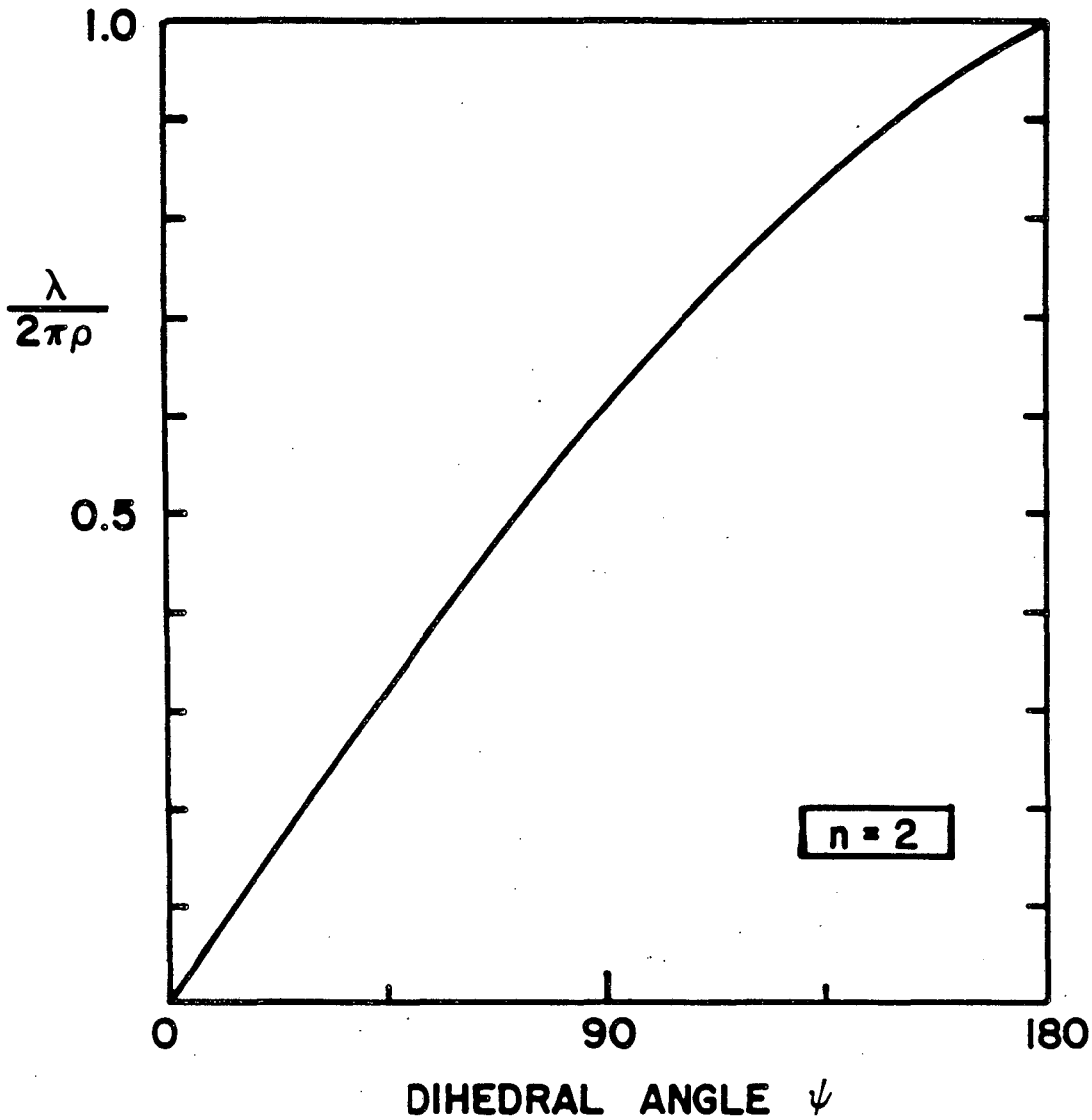

Figure 2c

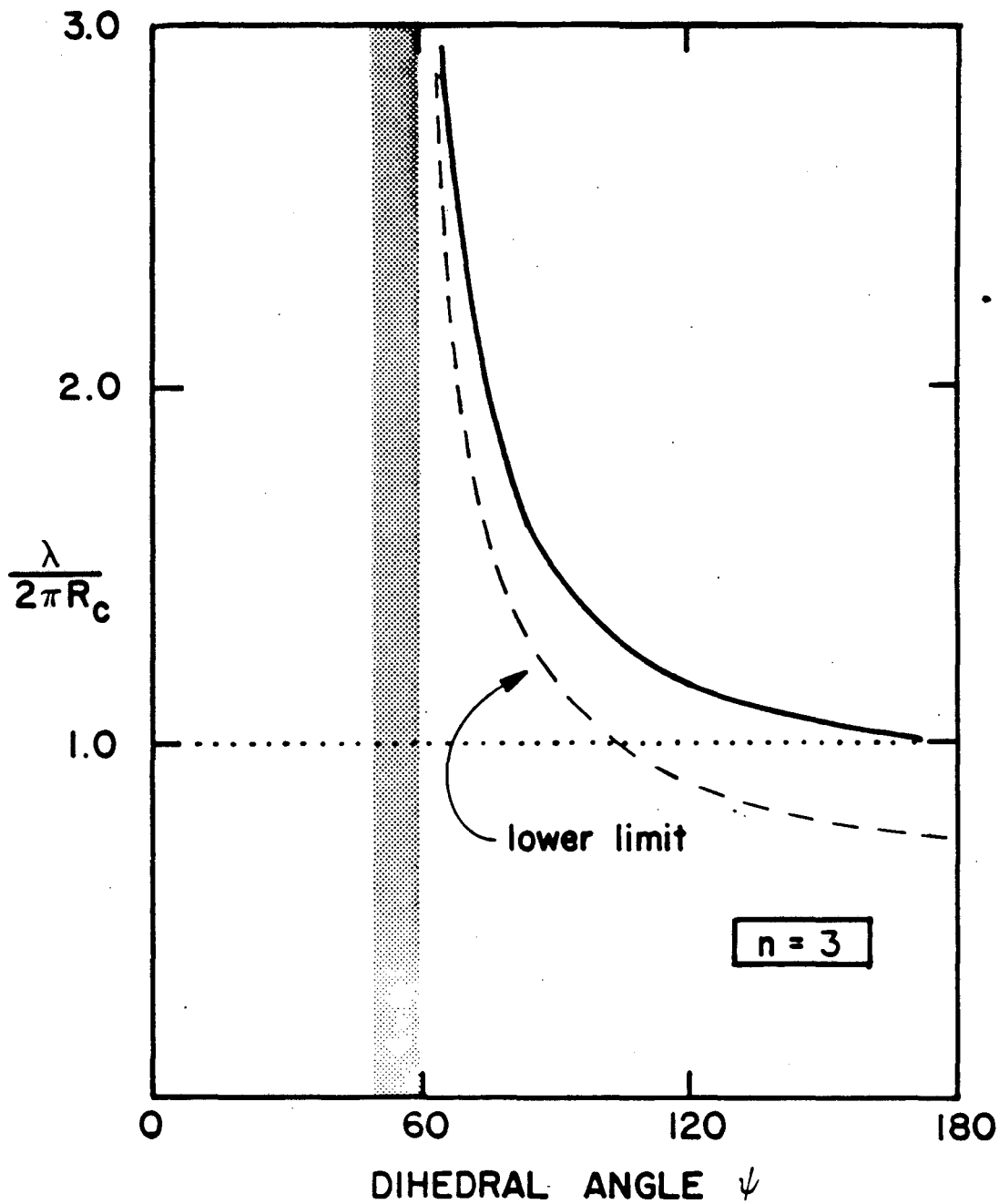
3.0
2.0
1.0
$\frac{\lambda}{2\pi R_c}$
lower limit
n = 3
0
60
120
180
DIHEDRAL ANGLE ψ

Figure 3a

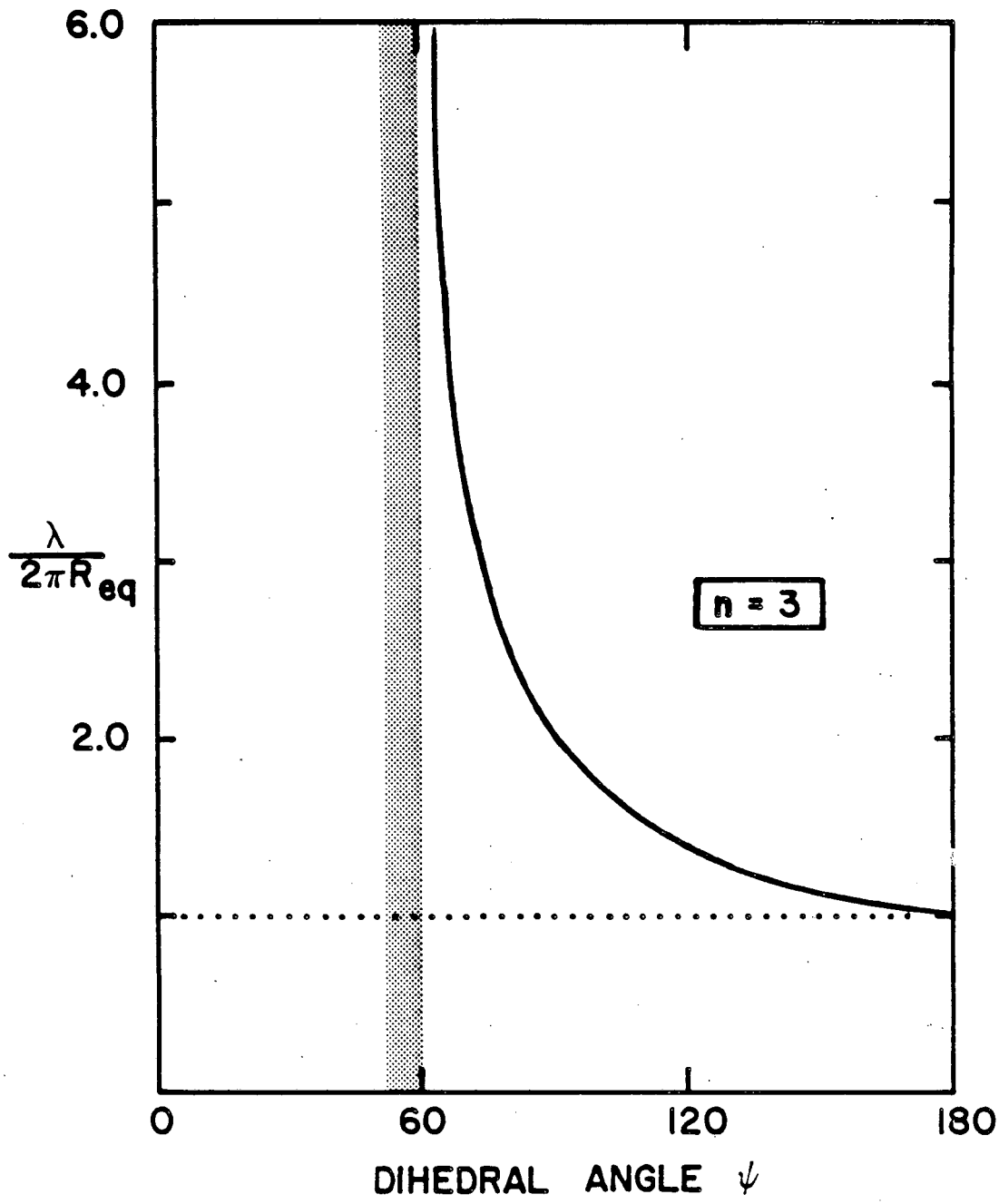

Figure 3b

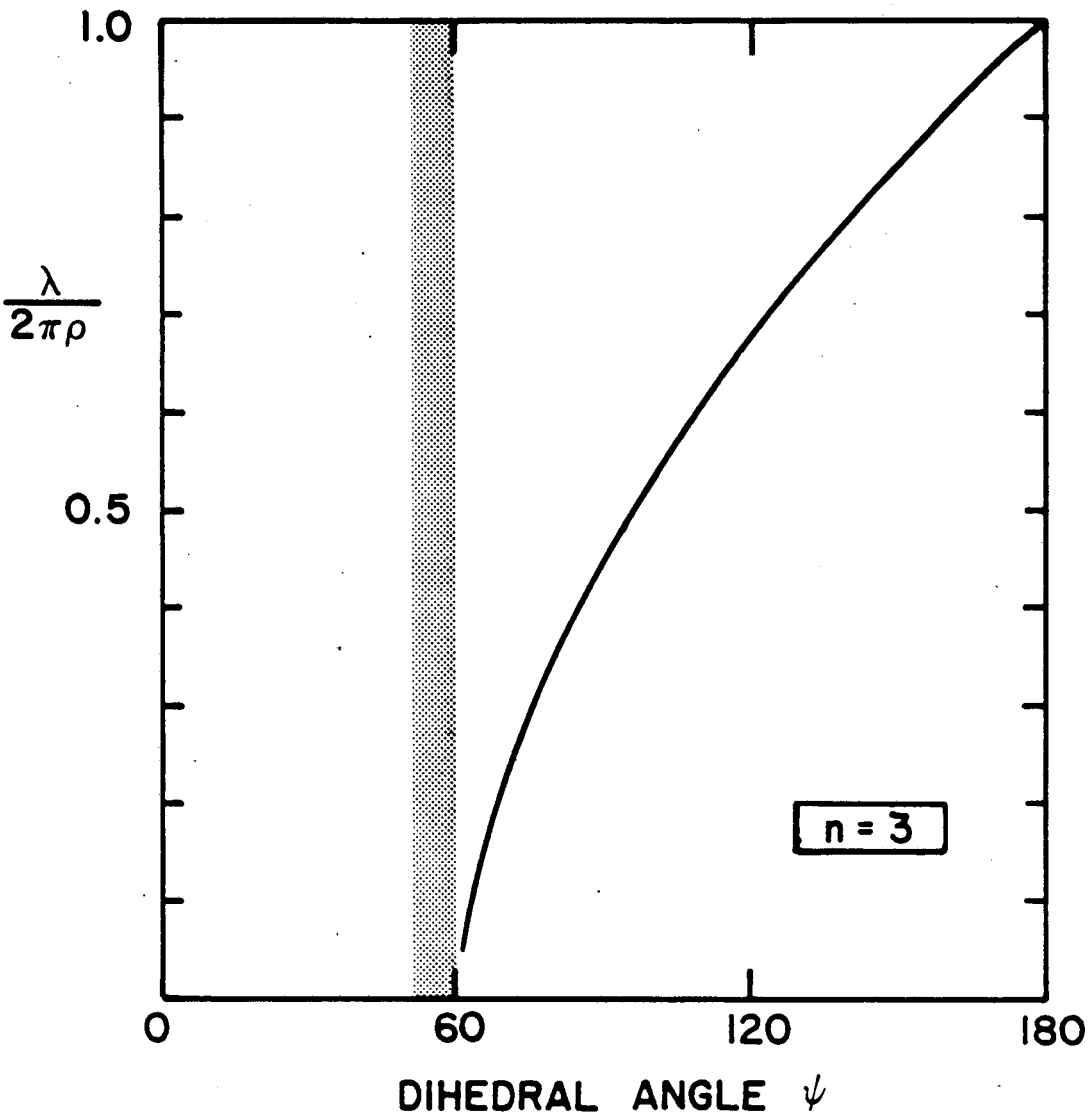

Figure 3c

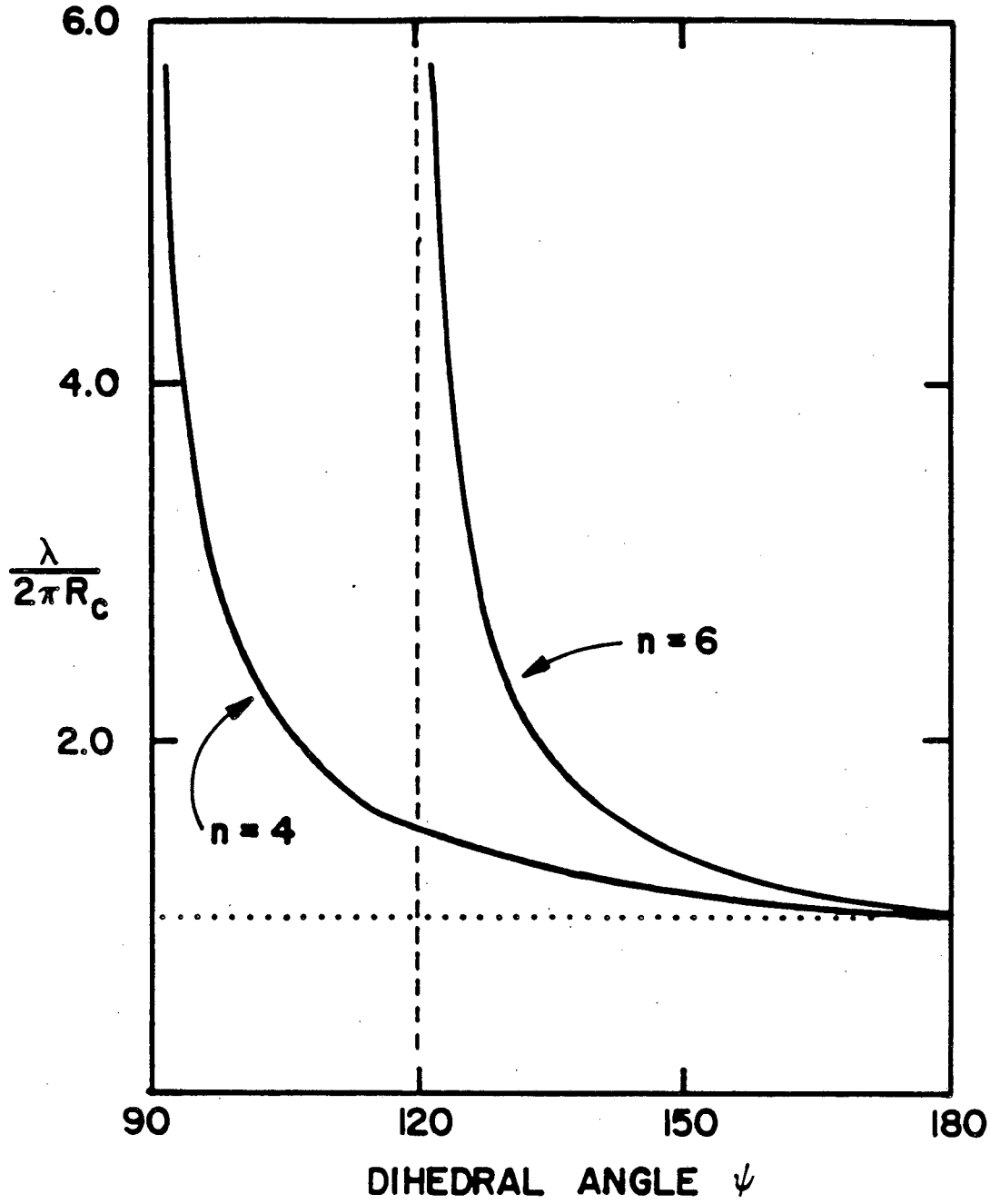
6.0
4.0
2.0
$\frac{\lambda}{2\pi R_c}$
n = 6
n = 4
90
120
150
180
DIHEDRAL ANGLE ψ

Figure 4a

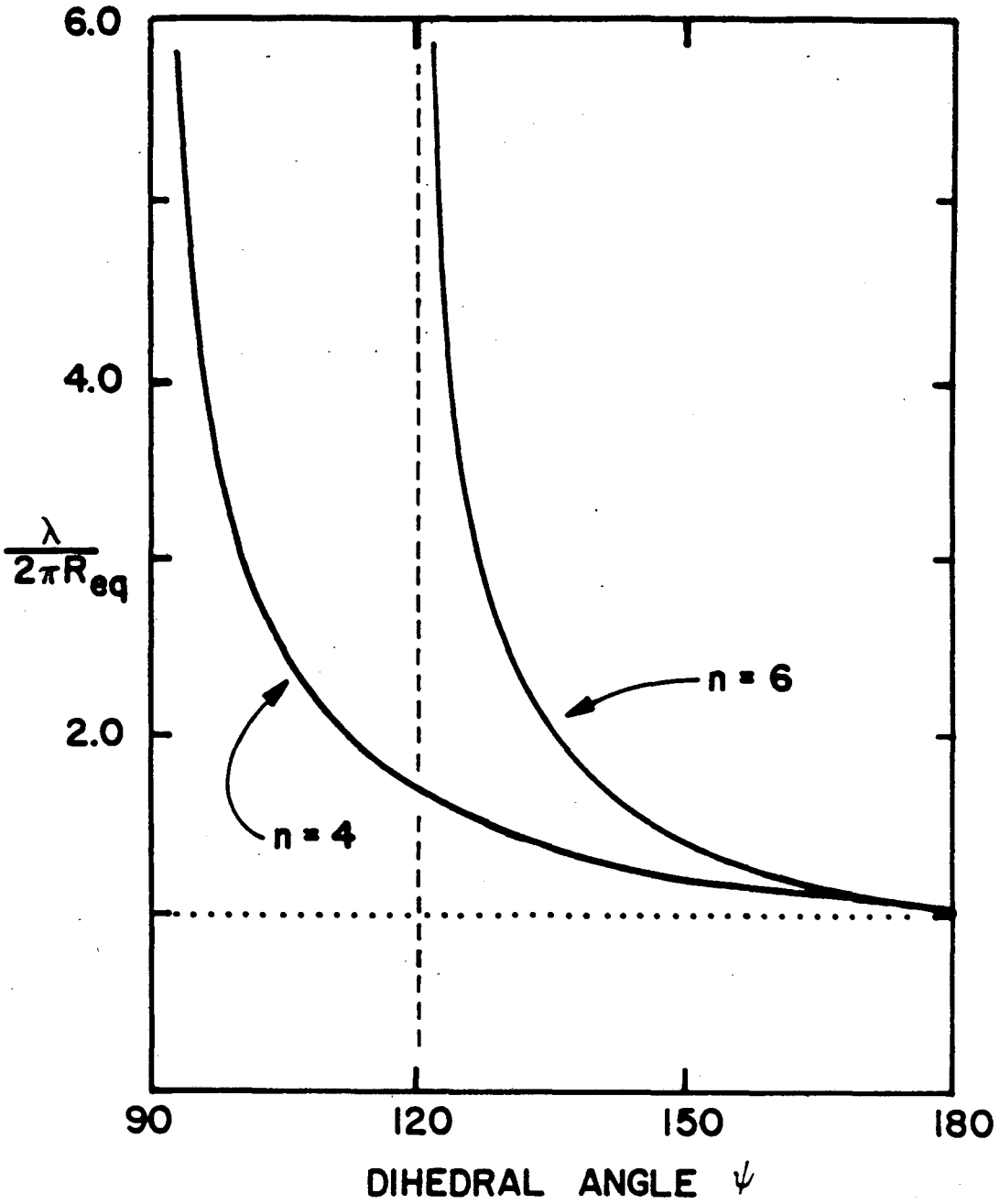
6.0
4.0
2.0
$\frac{\lambda}{2\pi R_{eq}}$
n = 6
n = 4
90
120
150
180
DIHEDRAL ANGLE ψ

Figure 4b

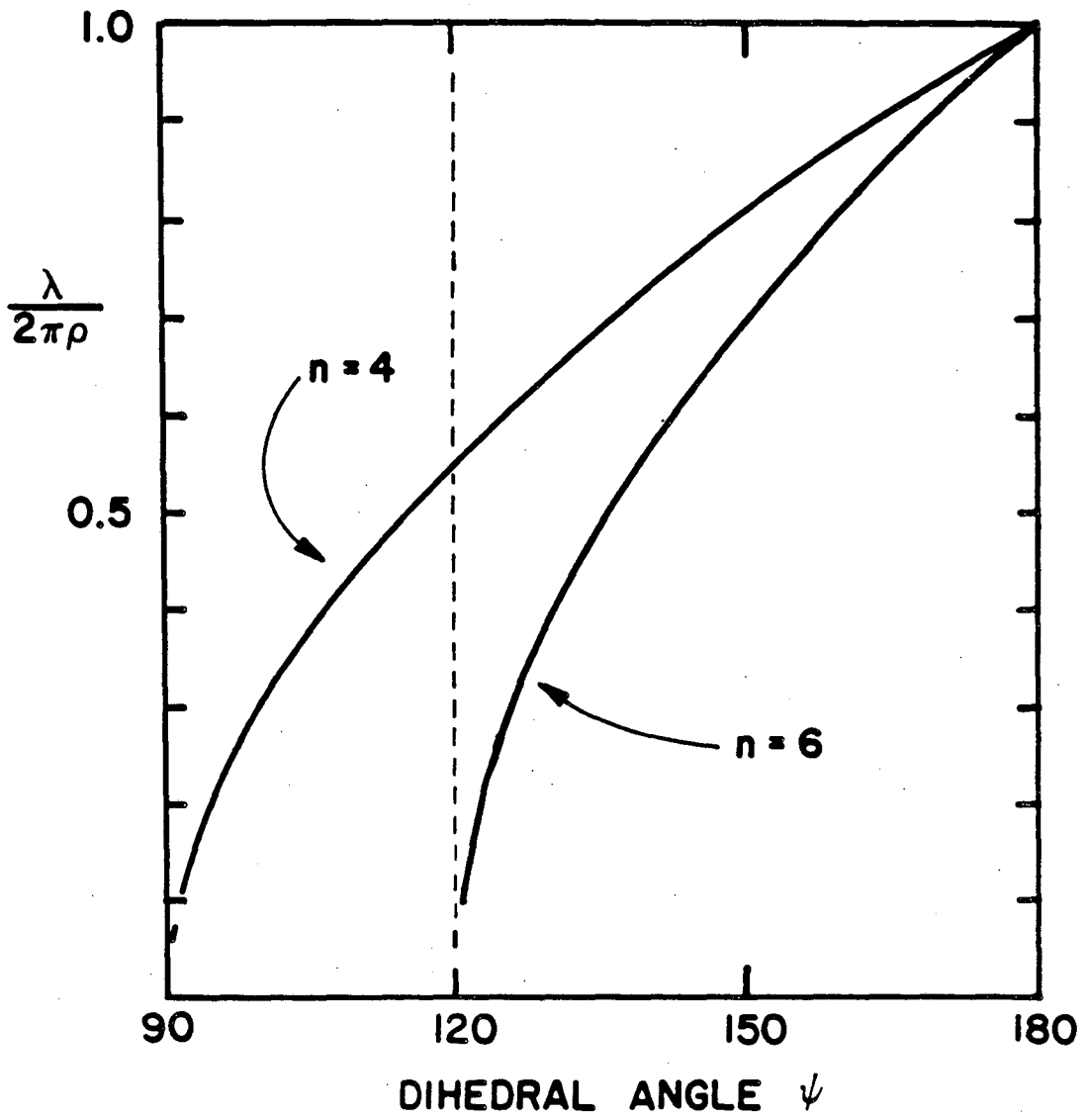
1.0
0.5
$\frac{\lambda}{2\pi\rho}$
n = 4
n = 6
90
120
150
180
DIHEDRAL ANGLE ψ

Figure 4c

This report was done with support from the Department of Energy. Any conclusions or opinions expressed in this report represent solely those of the author(s) and not necessarily those of The Regents of the University of California, the Lawrence Berkeley Laboratory or the Department of Energy.

Reference to a company or product name does not imply approval or recommendation of the product by the University of California or the U.S. Department of Energy to the exclusion of others that may be suitable.

LAWRENCE BERKELEY LABORATORY
TECHNICAL INFORMATION DEPARTMENT
UNIVERSITY OF CALIFORNIA
BERKELEY, CALIFORNIA 94720